Wave-equation migration velocity analysis — I: Theory

Geophysical Prospecting, accepted for publication

Paul Sava and Biondo Biondi

Stanford Exploration Project, Mitchell Bldg., Department of Geophysics,

Stanford University, Stanford, CA 94305-2215

(July 22, 2004)

ABSTRACT

We present a Migration Velocity Analysis (MVA) method based on wavefield extrapolation. Similar to conventional MVA, our method aims at iteratively improving the quality of the migrated image, as measured by flatness of Angle-Domain Common Image Gathers (ADCIG) over the aperture angle axis. However, instead of inverting the depth errors measured in ADCIGs using ray-based tomography, we invert "image perturbations" using a linearized wave-equation operator. This operator relates perturbations of the migrated image to perturbations of the migration velocity. We use prestack Stolt prestack residual migration to define the image perturbations that maximize focusing and flatness of ADCIGs.

Our linearized operator relates slowness perturbations to image perturbations based on a truncation of the Born scattering series to the first order term. To avoid divergence of the inversion procedure when the velocity perturbations are too large for the Born linearization of the wave-equation, we do not invert directly the image perturbations obtained by residual migration, but a linearized version of those image perturbations. The linearized image perturbations are computed by a linearized prestack residual migration operator applied to the background image. We illustrate with numeric examples

how the backprojection of those *linearized image perturbations*, i.e. the gradient of our objective function, is well behaved even in cases when backprojection of the original image perturbations would mislead the inversion and take it in the wrong direction.

In this paper, we demonstrate with simple synthetic examples that our method converges even when the starting velocity model is far from the correct one. In a companion paper (Sava and Biondi, 2004), we illustrate the full potential of our method in estimating velocity anomalies under complex salt bodies.

INTRODUCTION

Seismic imaging is a two-step process: velocity estimation and migration. As the velocity function becomes more complex, the two steps become more and more interdependent. In complex depth imaging problems, velocity estimation and migration are applied iteratively in a loop. To ensure that this iterative imaging process converges to a satisfactory model, it is crucial that the migration and the velocity estimation are consistent with each other.

Kirchhoff migration often fails in areas of complex geology, such as sub-salt, because the wavefield is severely distorted by lateral velocity variations leading to complex multipathing. As the shortcomings of Kirchhoff migration have become apparent (O'Brien and Etgen, 1998), there has been renewed interest in wave-equation migration and computationally efficient 3-D prestack depth migration methods have been developed (Biondi and Palacharla, 1996; Biondi, 1997; Mosher et al., 1997). However, no corresponding progress has been made in the development of Migration Velocity Analysis (MVA) methods based on the wave-equation. We aim at filling this gap by presenting a method that, at least in principle, can be used in conjunction with any downward-continuation migration method. In particular, we have been applying our new methodology to downward continuation

based on the Double Square Root (Yilmaz, 1979; Claerbout, 1985; Popovici, 1996) or common-azimuth (Biondi and Palacharla, 1996) equations.

As for migration, Wave-Equation MVA (WEMVA) is intrinsically more robust than ray-based MVA because it avoids the well-known instability problems that rays encounter when the velocity model is complex and has sharp boundaries. The transmission component of finite-frequency wave propagation is mostly sensitive to the smooth variations in the velocity model. Consequently, WEMVA produces smooth, stable velocity updates. In most cases, no smoothing constraints are needed to assure stability in the inversion. In contrast, ray-based methods require strong smoothing constraints to avoid divergence. These smoothing constraints often reduce the resolution of the inversion that would be otherwise possible given the characteristics of the data (e.g. geometry, frequency content, signal-to-noise ratio, etc.). Eliminating, or substantially reducing, the amount of smoothing increases the resolution of the final velocity model.

A well-known limitation of wave-equation tomography or MVA is represented by the linearization of the wave equation based on the truncation of the Born scattering series to the first order term. This linearization is hereafter referred to as the *Born approximation*. If the phase differences between the modeled and recorded wavefields are larger than a fraction of the wavelet, then the assumptions made under the Born approximation are violated and the velocity inversion methods diverge (Woodward, 1992; Pratt, 1999; Dahlen et al., 2000; Hung et al., 2000). Overcoming these limitations is crucial for a practical MVA tool. This goal is easier to accomplish with methods that optimize an objective function that is defined in the image space (e.g. DSO and our WEMVA) than with methods that optimize an objective function that is defined in the data space.

Our method employs the Born approximation to linearize the relationship between the velocity model and the image. However, we "manipulate" the image perturbations to assure that they are

consistent with the Born approximation, and replace the image perturbations with their linearized counterparts. We compute image perturbations by analytically linearizing our image-enhancement operator (e.g prestack residual migration) and applying this linearized operator to the background image. Therefore, the linearized image perturbations are approximations to the non-linear image perturbations that are caused by arbitrary changes of the velocity model. Since we linearize both operators (migration and residual migration) with respect to the amplitude of the images, the resulting linear operators are consistent with each other. Therefore, the inverse problem converges for a wider range of velocity anomalies than the one implied by the Born approximation.

Our method is more similar to conventional MVA than other proposed wave-equation methods for estimating the background velocity model (Noble et al., 1991; Bunks et al., 1995; Forgues et al., 1998) because it maximizes the migrated image quality instead of matching the recorded data directly. We define the quality of the migrated image by flatness of the migrated Angle-Domain Common Image Gathers (ADCIGs) along the aperture angle axis (Sava and Fomel, 2003). In this respect, our method is related to Differential Semblance Optimization (DSO) (Symes and Carazzone, 1991; Shen, 2003) and Multiple Migration Fitting (Chavent and Jacewitz, 1995). With respect to DSO, our method has the advantage that at each iteration it optimizes an objective function that rewards flatness in the ADCIGs globally (for all the angles at the same time), and not just locally as DSO does (minimizing the discrepancies between the image at each angle and the image at the adjacent angles). We suggest that this characteristic should speed-up the convergence, though we have no formal proof of our assertion.

This paper describes the theoretical foundations of wave-equation MVA with simple examples illustrating the main concepts and techniques. In a companion paper (Sava and Biondi, 2004), we present an application of wave-equation MVA to the challenging problem of velocity estimation under salt. Here, we begin by discussing wavefield scattering in the context of one-way wavefield

extrapolation methods. Next, we introduce the objective function for optimization and finally address the limitations introduced by the Born approximation. Two appendices detail the wave-equation MVA process and the computation of linearized image perturbations.

RECURSIVE WAVEFIELD EXTRAPOLATION

Imaging by wavefield extrapolation (WE) is based on recursive continuation of the wavefields ($\mathcal{U}$) from a given depth level to the next by means of an extrapolation operator ($\mathbf{E}$):

$$\mathcal{U}_{z+\Delta z} = \mathbf{E}_z \left[\mathcal{U}_z \right] . \tag{1}$$

Here and hereafter, we use the following notation conventions: $\mathbf{A}[x]$ means operator $\mathbf{A}$ applied to x, and $f(x)$ means function f of argument x. The subscripts z or $z+\Delta z$ indicate quantities corresponding to the depth levels z and $z+\Delta z$, respectively.

This recursive equation (1) can also be explicitly written in matrix form as

$$\begin{pmatrix} \mathbf{1} & \mathbf{0} & \mathbf{0} & \cdots & \mathbf{0} & \mathbf{0} \\ -\mathbf{E}_0 & \mathbf{1} & \mathbf{0} & \cdots & \mathbf{0} & \mathbf{0} \\ \mathbf{0} & -\mathbf{E}_1 & \mathbf{1} & \cdots & \mathbf{0} & \mathbf{0} \\ \vdots & \vdots & \vdots & \vdots & \vdots & \vdots \\ \mathbf{0} & \mathbf{0} & \mathbf{0} & \cdots & -\mathbf{E}_{n-1} & \mathbf{1} \end{pmatrix} \begin{pmatrix} \mathcal{U}_0 \\ \mathcal{U}_1 \\ \mathcal{U}_2 \\ \vdots \\ \mathcal{U}_n \end{pmatrix} = \begin{pmatrix} \mathcal{D}_0 \\ 0 \\ 0 \\ \vdots \\ 0 \end{pmatrix},$$

or in a more compact notation as:

$$(\mathbf{1} - \mathbf{E})\, \mathcal{U} = \mathcal{D}, \tag{2}$$

where the vector $\mathcal{D}$ stands for data, $\mathcal{U}$ for the extrapolated wavefield at all depth levels, $\mathbf{E}$ for the extrapolation operator and $\mathbf{1}$ for the identity operator. Here and hereafter, we make the distinction between quantities measured at a particular depth level (e.g. $\mathcal{U}_z$), and the corresponding vectors denoting such quantities at all depth levels (e.g. $\mathcal{U}$).

After wavefield extrapolation, we obtain an image by applying, at every depth level, an imaging

operator ($\mathbf{I}_z$) to the extrapolated wavefield $\mathcal{U}_z$:

$$\mathcal{R}_z = \mathbf{I}_z \left[\mathcal{U}_z \right] , \tag{3}$$

where $\mathcal{R}_z$ stands for the image at some depth level. A commonly used imaging operator ($\mathbf{I}_z$) involves summation over the temporal frequencies. We can write the same relation in compact matrix form as:

$$\mathcal{R} = \mathbf{I}\mathcal{U} . \tag{4}$$

$\mathcal{R}$ stands for the image, and $\mathbf{I}$ stands for the imaging operator which is applied to the extrapolated wavefield $\mathcal{U}$ at all depth levels.

A perturbation of the wavefield at some depth level can $\Delta\mathcal{U}$ be derived from the background wavefield by a simple application of the chain rule of derivation to equation (1):

$$\Delta\mathcal{U}_{z+\Delta z} = \mathbf{E}_z \left[\Delta\mathcal{U}_z \right] + \Delta\mathcal{V}_{z+\Delta z} , \tag{5}$$

where $\Delta\mathcal{V}_{z+\Delta z} = \Delta\mathbf{E}_z \left[\mathcal{U}_z \right]$ represents the scattered wavefield generated at $z+\Delta z$ by the interaction of the wavefield $\mathcal{U}_z$ with a perturbation of the velocity model at depth z. $\Delta\mathcal{U}_{z+\Delta z}$ is the accumulated wavefield perturbation corresponding to slowness perturbations at all levels above. It is computed by extrapolating the wavefield perturbation from the level above $\Delta\mathcal{U}_z$, plus the scattered wavefield at this level $\Delta\mathcal{V}_{z+\Delta z}$.

Equation (5) is also a recursive equation which can be written in matrix form as

$$\begin{pmatrix} \mathbf{1} & \mathbf{0} & \mathbf{0} & \cdots & \mathbf{0} & \mathbf{0} \\ -\mathbf{E}_0 & \mathbf{1} & \mathbf{0} & \cdots & \mathbf{0} & \mathbf{0} \\ \mathbf{0} & -\mathbf{E}_1 & \mathbf{1} & \cdots & \mathbf{0} & \mathbf{0} \\ \vdots & \vdots & \vdots & \vdots & \vdots & \vdots \\ \mathbf{0} & \mathbf{0} & \mathbf{0} & \cdots & -\mathbf{E}_{n-1} & \mathbf{1} \end{pmatrix} \begin{pmatrix} \Delta\mathcal{U}_0 \\ \Delta\mathcal{U}_1 \\ \Delta\mathcal{U}_2 \\ \vdots \\ \Delta\mathcal{U}_n \end{pmatrix} = \begin{pmatrix} \mathbf{0} & \mathbf{0} & \mathbf{0} & \cdots & \mathbf{0} & \mathbf{0} \\ \Delta\mathbf{E}_0 & \mathbf{0} & \mathbf{0} & \cdots & \mathbf{0} & \mathbf{0} \\ \mathbf{0} & \Delta\mathbf{E}_1 & \mathbf{0} & \cdots & \mathbf{0} & \mathbf{0} \\ \vdots & \vdots & \vdots & \vdots & \vdots & \vdots \\ \mathbf{0} & \mathbf{0} & \mathbf{0} & \cdots & \Delta\mathbf{E}_{n-1} & \mathbf{0} \end{pmatrix} \begin{pmatrix} \mathcal{U}_0 \\ \mathcal{U}_1 \\ \mathcal{U}_2 \\ \vdots \\ \mathcal{U}_n \end{pmatrix},$$

or in a more compact notation as:

$$(\mathbf{1} - \mathbf{E})\,\Delta\mathcal{U} = \Delta\mathbf{E}\mathcal{U}. \tag{6}$$

The operator $\Delta\mathbf{E}$ stands for a perturbation of the extrapolation operator $\mathbf{E}$. The quantity $\Delta\mathbf{E}\mathcal{U}$ represents a scattered wavefield, and is a function of the perturbation in the medium by the scattering relations derived in Appendix A. For the case of single scattering, we can write that

$$\Delta\mathcal{V}_{z+\Delta z} \equiv \Delta\mathbf{E}_z\left[\mathcal{U}_z\right] = \mathbf{E}_z\left[\mathbf{S}_z\left(\widetilde{\mathcal{U}}_z\right)\left[\Delta s_z\right]\right]. \tag{7}$$

The expression for the total wavefield perturbation $\Delta\mathcal{U}$ from equation (5) becomes

$$\Delta\mathcal{U}_{z+\Delta z} = \mathbf{E}_z\left[\Delta\mathcal{U}_z\right] + \mathbf{E}_z\left[\mathbf{S}_z\left(\widetilde{\mathcal{U}}_z\right)\left[\Delta s_z\right]\right], \tag{8}$$

which is also a recursive relation that can be written in matrix form as

$$\begin{pmatrix} \mathbf{1} & \mathbf{0} & \mathbf{0} & \cdots & \mathbf{0} & \mathbf{0} \\ -\mathbf{E}_0 & \mathbf{1} & \mathbf{0} & \cdots & \mathbf{0} & \mathbf{0} \\ \mathbf{0} & -\mathbf{E}_1 & \mathbf{1} & \cdots & \mathbf{0} & \mathbf{0} \\ \vdots & \vdots & \vdots & \vdots & \vdots & \vdots \\ \mathbf{0} & \mathbf{0} & \mathbf{0} & \cdots & -\mathbf{E}_{n-1} & \mathbf{1} \end{pmatrix} \begin{pmatrix} \Delta\mathcal{U}_0 \\ \Delta\mathcal{U}_1 \\ \Delta\mathcal{U}_2 \\ \vdots \\ \Delta\mathcal{U}_n \end{pmatrix} = \begin{pmatrix} \mathbf{0} & \mathbf{0} & \mathbf{0} & \cdots & \mathbf{0} & \mathbf{0} \\ \mathbf{E}_0 & \mathbf{0} & \mathbf{0} & \cdots & \mathbf{0} & \mathbf{0} \\ \mathbf{0} & \mathbf{E}_1 & \mathbf{0} & \cdots & \mathbf{0} & \mathbf{0} \\ \vdots & \vdots & \vdots & \vdots & \vdots & \vdots \\ \mathbf{0} & \mathbf{0} & \mathbf{0} & \cdots & \mathbf{E}_{n-1} & \mathbf{0} \end{pmatrix} \begin{pmatrix} \mathbf{S}_0 & \mathbf{0} & \mathbf{0} & \cdots & \mathbf{0} \\ \mathbf{0} & \mathbf{S}_1 & \mathbf{0} & \cdots & \mathbf{0} \\ \mathbf{0} & \mathbf{0} & \mathbf{S}_2 & \cdots & \mathbf{0} \\ \vdots & \vdots & \vdots & \vdots & \vdots \\ \mathbf{0} & \mathbf{0} & \mathbf{0} & \cdots & \mathbf{S}_n \end{pmatrix} \begin{pmatrix} \Delta s_0 \\ \Delta s_1 \\ \Delta s_2 \\ \vdots \\ \Delta s_n \end{pmatrix},$$

or in a more compact notation as:

$$(\mathbf{1}-\mathbf{E})\,\Delta\mathcal{U} = \mathbf{E}\mathbf{S}\Delta s. \tag{9}$$

The vector Δs stands for the slowness perturbation at all depths.

Finally, if we introduce the notation

$$\mathbf{G} = (\mathbf{1}-\mathbf{E})^{-1}\,\mathbf{E}\mathbf{S}, \tag{10}$$

we can write a simple relation between a slowness perturbation Δs and the corresponding wavefield perturbation $\Delta\mathcal{U}$:

$$\Delta\mathcal{U} = \mathbf{G}\Delta s. \tag{11}$$

This expression describes wavefield scattering caused by the interaction of the background wavefield with a perturbation of the medium.

MIGRATION VELOCITY ANALYSIS

Migration velocity analysis is based on estimating the velocity that optimizes certain properties of the migrated images. In general, measuring such properties involves making a transformation after wavefield extrapolation to the migrated image using a function f

$$\mathcal{P}_z = f\mathbf{I}_z\left[\mathcal{U}_z\right], \tag{12}$$

where $\mathbf{I}$ is the imaging operator applied to the extrapolated wavefield $\mathcal{U}$. In compact matrix form, we can write this relation as:

$$\mathcal{P} = f\left(\mathbf{I}\mathcal{U}\right) . \tag{13}$$

The image $\mathcal{P}$ is subject to optimization from which we derive the velocity updates.

Two examples of transformation functions are:

- $f(x) = x - t$ where t is a known target. A WEMVA method based on this criterion optimizes

$$\mathcal{P}_z = \mathbf{I}_z\left[\mathcal{U}_z\right] - \mathbf{I}_z\left[\mathcal{T}_z\right] , \tag{14}$$

  where $\mathcal{T}_z$ stands for the target wavefield. For this method, we can use the acronym TIF standing for *target image fitting* (Biondi and Sava, 1999; Sava and Fomel, 2002).

- $f(x) = Dx$ where D is a known operator. A WEMVA method based on this criterion optimizes

$$\mathcal{P}_z = \mathbf{D}_z\left[\mathbf{I}_z\left[\mathcal{U}_z\right]\right]. \tag{15}$$

  If $\mathbf{D}$ is a differential semblance operator, we can use the acronym DSO standing for *differential semblance optimization* (Symes and Carazzone, 1991; Shen, 2003).

In general, such transformations belong to a family of affine functions that can be written as

$$\mathcal{P}_z = \mathbf{A}_z\left[\mathbf{I}_z\left[\mathcal{U}_z\right]\right] - \mathbf{B}_z\left[\mathbf{I}_z\left[\mathcal{T}_z\right]\right], \tag{16}$$

or in compact matrix form as

$$\mathcal{P} = \mathbf{AI}\mathcal{U} - \mathbf{BI}\mathcal{T}, \tag{17}$$

where the operators $\mathbf{A}$ and $\mathbf{B}$ are known and take special forms depending on the optimization criterion we use. For example, $\mathbf{A} = \mathbf{1}$ and $\mathbf{B} = \mathbf{1}$ for TIF, and $\mathbf{A} = \mathbf{D}$ and $\mathbf{B} = \mathbf{0}$ for DSO. $\mathbf{1}$ stands for the identity operator, and $\mathbf{0}$ stands for the null operator. With the definition in equation (16), we can write the objective function J as:

$$\begin{aligned} J(s) &= \frac{1}{2}\sum_{z,\mathbf{m},\mathbf{h}} |\mathcal{P}_z|^2 & (18)\\ &= \frac{1}{2}\sum_{z,\mathbf{m},\mathbf{h}} \left|\mathbf{A}_z\left[\mathbf{I}_z\left[\mathcal{U}_z\right]\right] - \mathbf{B}_z\left[\mathbf{I}_z\left[\mathcal{T}_z\right]\right]\right|^2 , & (19) \end{aligned}$$

where s is the slowness function, and $z, \mathbf{m}, \mathbf{h}$ stand respectively for depth, and the midpoint and offset vectors. In compact matrix form, we can write the objective function as:

$$J(s) = \frac{1}{2}\left|\mathbf{AI}\mathcal{U} - \mathbf{BI}\mathcal{T}\right|^2 . \tag{20}$$

In the Born approximation, the total wavefield $\mathcal{U}$ is related to the background wavefield $\widetilde{\mathcal{U}}$ by the linear relation

$$\mathcal{U} \approx \widetilde{\mathcal{U}} + \mathbf{G}\Delta s . \tag{21}$$

If we can replace the total wavefield in the objective function equation (20), we obtain

$$J(s) = \frac{1}{2}\left|\mathbf{AI}\widetilde{\mathcal{U}} - \mathbf{BI}\mathcal{T} + \mathbf{AIG}\Delta s\right|^2 . \tag{22}$$

Equation (22) describes a linear optimization problem, where we obtain Δs by minimizing the objective function

$$J(\Delta s) = \left|\Delta\mathcal{R} - \mathbf{L}\Delta s\right|^2 , \tag{23}$$

where $\Delta\mathcal{R} = -\left(\mathbf{AI}\widetilde{\mathcal{U}} - \mathbf{BI}\mathcal{T}\right)$, and $\mathbf{L} = \mathbf{AIG}$. The operator $\mathbf{L}$ is constructed based on the Born approximation (Lo and Inderweisen, 1994), and involves the pre-computed background wavefield

through the background medium. A discussion on the implementation details for operator $\mathbf{L}$ is presented in Appendix A. The convex optimization problem defined by the linearization in equation (22) can be solved using standard conjugate-gradient techniques.

Since, in most practical cases, the inversion problem is not well conditioned, we need to add constraints on the slowness model via a regularization operator. In these situations, we use the modified objective function

$$J(\Delta s) = |\Delta\mathcal{R} - \mathbf{L}\Delta s|^2 + \epsilon^2 |\mathbf{A}\Delta s|^2 \ . \tag{24}$$

Here, $\mathbf{A}$ is a regularization operator, and ϵ is a scalar parameter which balances the relative importance of the data residual ($\Delta\mathcal{R} - \mathbf{L}\Delta s$) and the model residual ($\mathbf{A}\Delta s$).

We illustrate our method with a simple model depicted in Figure 1. The velocity is constant and the data are represented by an impulse in space and time. We consider two slowness models: one regarded as the correct slowness s_c, and the other as the background slowness $\tilde{s}$. The two slownesses are related by a scale factor $\frac{s_c}{\tilde{s}} = \rho$. For this example, we consider $\rho = 1.001$ to ensure that we do not violate the requirements imposed by the Born approximation.

Next, we migrate the data with the background slowness $\tilde{s}$ and store the extrapolated wavefield at all depth levels. Figure 1a shows the image corresponding to the background slowness $\widetilde{\mathcal{R}}$. We also migrate the data with the correct slowness and obtain a second image $\mathcal{R}_c$. A simple subtraction of the two images gives the image perturbation in Figure 1b.

Finally, we compute an image perturbation by a simple application of the forward WEMVA operator defined in equation (23) to the slowness perturbation $\Delta s = s_c - \tilde{s}$ (Figure 1c). Since the slowness perturbation is very small, the requirements imposed by the Born approximation are fulfilled, and the two images in Figures 1b and 1c are identical. The image perturbations are phase-shifted by 90° relative to the background image.

A simple illustration of the adjoint operator $\mathbf{L}$ defined in equation (23) is depicted in Figure 2. Panel (a) shows the background image, panels (b) and (c) show image perturbations, and panels (d) and (e) show slowness perturbations. We extract a small subset of each image perturbation to create the impulsive image perturbations in Figures 2b and 2c. The left panels (b and d) correspond to the image perturbation computed as an image difference, while the panels on the right (c and e) correspond to the image perturbation computed with the forward WEMVA operator. In this way, our data corresponds to a single point on the surface, and our image perturbation corresponds to a single point in the subsurface. By backprojecting the image perturbations in Figures 2b and 2c with the adjoint WEMVA operator, we obtain identical "fat rays" shown in Figures 2d and 2e, respectively.

IMAGE PERTURBATION BY RESIDUAL MIGRATION

Prestack Stolt Residual Migration (PSRM) can be used to create image perturbations (Sava, 2003). Given an image migrated with the background velocity, we can construct another image by using an operator $\mathbf{K}$ function of a parameter ρ which represents the ratio of the original and modified velocities. The improved velocity map is unknown explicitly, although it is described indirectly by the ratio map of the two velocities:

$$\mathcal{R} = \mathbf{K}(\rho)\left[\widetilde{\mathcal{R}}\right] . \tag{25}$$

The simplest form of an image perturbation can be constructed as a difference between an *improved* image ($\mathcal{R}$) and the *background* image ($\widetilde{\mathcal{R}}$):

$$\Delta\mathcal{R} = \mathcal{R} - \widetilde{\mathcal{R}} . \tag{26}$$

The main challenge with this method of constructing image perturbations for WEMVA is that the two images can be phase-shifted too much with respect to one-another. Thus, we violate the requirements

of the Born approximation and risk subtracting images that are out of phase. This problem is common for all wavefield-based velocity analysis or tomographic methods using the Born approximation (Woodward, 1992; Pratt, 1999; Dahlen et al., 2000).

A simple illustration of this problem is depicted in Figures 3 and 4. This example is similar with the one in Figures 1 and 2, except that the velocity ratio linking the two slownesses is much larger: $\rho = 1.20$. In this case, the background and correct images are not at all in phase, and when we subtract them we obtain two distinct events, as shown in Figure 3b. In contrast, the image perturbation obtained by the forward WEMVA operator, Figure 3c, shows only one event as in the previous example. The only difference between the image perturbations in Figures 1c and 3c is a scale factor related to the magnitude of the slowness anomaly.

Figure 4 depicts fat rays for each kind of image perturbation: on the left, the image perturbations obtained by subtraction of the two images, and on the right, the image perturbation obtained with the forward WEMVA operator. The fat rays corresponding to the ideal image perturbation (panels c and e) do not change from the previous example, except for a scale factor. However, in case we use image differences (panels b and d), we violate the requirements of the Born approximation. In this case, we see slowness backprojections of opposite sign relative to the true anomaly, and we also see the two characteristic migration ellipsoidal side-events indicating cycle-skipping (Woodward, 1992).

We address this problem by employing linearized image perturbations. If we define $\Delta\rho = \rho - 1$, we can write a discrete version of the image perturbation using a Taylor series expansion of equation (25) as

$$\Delta\mathcal{R} \approx \mathbf{K}^{'}\Big|_{\rho=1}\left[\widetilde{\mathcal{R}}\right]\Delta\rho\,, \tag{27}$$

where the $'$ sign denotes derivation relative to the velocity ratio parameter ρ. For the image perturbations computed with equation (27), we use the name *linearized image perturbations*. Figure 5

graphically illustrates this procedure.

The linearized PSRM operator $\mathbf{K}^{'}\big|_{\rho=1}$ can be computed analytically, as described in Appendix B. With this operator, we can compute linearized image perturbations in two steps. First, we run residual migration for a large range of velocity ratios and pick at every image point the ratio which maximizes flatness of the gathers. Then, we apply the operator in equation (27) to the background image $\widetilde{\mathcal{R}}$ and scale the result with the picked $\Delta\rho$.

The linearized image perturbations approximate the non-linear image perturbations caused by arbitrary velocity model changes. They are based on the gradient of the image change relative to a velocity model change, and are less restrictive than the Born approximation limits.

Figure 6 shows how the linearized image perturbation methodology applies to the synthetic example used earlier in this paper. All panels are similar to the ones in Figures 2 and 4, except that the left panels (b and d) correspond to linearized image perturbations, instead of simple image perturbations. Again, we compare image and slowness perturbations with the ideal perturbations obtained by the forward WEMVA operator (c and e). Both the image and slowness perturbations are identical in shape and magnitude.

Inversion example

Our next example concerns linearized image perturbations computed for prestack images. We use another simple model with flat reflectors and constant velocity. The image perturbation methodology is identical to the one outlined in the preceding paragraphs. The main point of this example is to illustrate our methodology in a situation when the requirements of the first-order Born approximation are clearly violated. In this case, the slowness perturbation is 50% of the background slowness.

Figure 7 shows representative common-image gathers in the angle-domain (Sava and Fomel,

2003) for the background image (a), the correct image (b), the image perturbation obtained as a difference of the two images (c), the image perturbation obtained using the forward WEMVA operator (d), and the linearized image perturbation (e). Panels (d) and (e) are identical within numeric precision, indicating that our methodology can successfully be employed to create correct image perturbations well beyond the limits of the first-order Born approximation.

Finally, we apply our migration velocity analysis algorithm to the example in Figure 7. First, we compute the background wavefield represented by the background image (Figures 7a and 8a). Next, we compute the linearized image perturbation, shown in Figure 9a (stack) and in Figure 7e (angle gather from the middle of the image).

From this image perturbation, we invert for the slowness perturbation (Figure 9b). We stop the inversion after 19 linear iterations when the data residual has stopped decreasing (Figure 9c). The slowness updates occur in the upper half of the model. Since no reflectors exist in the bottom part of the model, no slowness update is computed for this region.

Finally, we remigrate the data using the updated slowness and obtain the image in Figure 8b. For comparison, Figure 8c depicts the image obtained after migration with the correct slowness. The two images are identical in the upper half where we have updated the slowness model. Further updates to the model would require more non-linear iterations.

CONCLUSION

We present a new migration velocity analysis method using wavefield-extrapolation techniques that can address the challenges posed by velocity estimation in complicated media with sharp contrasts and fine-scale features. Our method is formulated in the migrated image space, with an objective function aimed at improving the image quality. The method is based on a linearization of the down-

ward continuation operator that relates perturbations of slowness models to perturbations of migrated images. Since our method is based on finite-difference extrapolation of band-limited waves, it naturally takes into account the multipathing that characterizes wave propagation in complex environments with large and sharp velocity contrasts. It also takes into account the full wavefield information, and not only selectively picked traveltimes, as it is currently done in state-of-the-art traveltime tomography.

We use prestack Stolt residual migration to define image perturbations by maximizing focusing and flatness of angle-domain common-image gathers. In general, the image perturbations computed with this method can be too different from the background image, and we are in danger of subtracting images that are not in phase, violating our first-order Born approximation assumption. We avoid divergence of the inversion procedure when the velocity perturbations are too large, by not inverting directly the image perturbations obtained by residual migration, but by inverting linearized versions of them. Thus, we achieve a method which is robust with respect to large model perturbations, a crucial step for a practical MVA method.

We illustrate our method with simple numeric examples, and show that our method is well behaved even for large slowness perturbations, well beyond the limits of the first-order Born approximation. A companion paper (Sava and Biondi, 2004) illustrates the full potential of our method with more complex examples.

ACKNOWLEDGMENT

We would like to acknowledge the financial support of the sponsors of Stanford Exploration Project.

REFERENCES

Biondi, B., 1997, Azimuth moveout + common-azimuth migration: Cost-effective prestack depth imaging of marine data *in* 67th Ann. Internat. Mtg. Soc. of Expl. Geophys., 1375–1378.

Biondi, B., and Palacharla, G., 1996, 3-D prestack migration of common-azimuth data: Geophysics, **61**, 1822–1832.

Biondi, B., and Sava, P., 1999, Wave-equation migration velocity analysis: 69th Ann. Internat. Meeting, Soc. of Expl. Geophys., Expanded Abstracts, 1723–1726.

Bunks, C., Saleck, F. M., Zaleski, S., and Chavent, G., 1995, Multiscale seismic waveform inversion: Geophysics, **60**, 1457–1473.

Chavent, G., and Jacewitz, C. A., 1995, Determination of background velocities by multiple migration fitting: Geophysics, **60**, 476–490.

Claerbout, J. F., 1985, Imaging the Earth's Interior: Blackwell Scientific Publications.

Dahlen, F. A., Hung, S. H., and Nolet, G., 2000, Frechet kernels for finite frequency traveltimes—I. Theory: Geophys. J. Int., **141**, 157–174.

Forgues, E., Scala, E., and Pratt, R. G., 1998, High resolution velocity model estimation from refraction and reflection data *in* 68th Ann. Internat. Mtg. Soc. of Expl. Geophys., 1211–1214.

de Hoop, M., le Rousseau, J. H., and Wu, R. S., 1996, Generalization of the phase-screen approximation for the scattering of acoustic waves: Wave Motion, **31**, 43–70.

Huang, L. Y., Fehler, M. C., and Wu, R. S., 1999, Extended local Born Fourier migration method: Geophysics, **64**, 1524–1534.

Hung, S. H., Dahlen, F. A., and Nolet, G., 2000, Frechet kernels for finite frequency traveltimes—II. Examples: Geophys. J. Int., **141**, 175–203.

Lo, T. W., and Inderweisen, P. L., 1994, Fundamentals of Seismic Tomography: Soc. of Expl. Geophys.

Mosher, C. C., Foster, D. J., and Hassanzadeh, S., 1997, Common angle imaging with offset plane waves *in* 67th Ann. Internat. Mtg. Soc. of Expl. Geophys., 1379–1382.

Noble, M., Lindgren, J., and Tarantola, A., 1991, Large-sized, nonlinear inversion of a marine data set: Retrieving the source, the background velocity and the impedance contrasts *in* 61st Ann. Internat. Mtg. Soc. of Expl. Geophys., 893–896.

O'Brien, M. J., and Etgen, J. T., 1998, Wavefield imaging of complex structures with sparse, point-receiver data *in* 68th Ann. Internat. Mtg. Soc. of Expl. Geophys., 1365–1368.

Popovici, A. M., 1996, Prestack migration by split-step DSR: Geophysics, **61**, 1412–1416.

Pratt, R. G., 1999, Seismic waveform inversion in the frequency domain, Part 1: Theory and verification in a physical scale model: Geophysics, **64**, 888–901.

Ristow, D., and Ruhl, T., 1994, Fourier finite-difference migration: Geophysics, **59**, 1882–1893.

Sava, P., 2003, Prestack residual migration in the frequency domain: Geophysics, **67**, 634–640.

Sava, P., and Biondi, B., 2004, Wave-equation migration velocity analysis—II: Examples: Geophysical Prospecting, submitted for publication.

Sava, P., and Fomel, S., 2002, Wave-equation migration velocity analysis beyond the Born approximation: 72nd Ann. Internat. Mtg., Soc. of Expl. Geophys., Expanded Abstracts, 2285–2288.

—, 2003, Angle-domain common image gathers by wavefield continuation methods: Geophysics, **68**, 1065–1074.

Shen, P., 2003, Differential semblance velocity analysis by wave-equation migration *in* 73rd Ann. Internat. Mtg. Soc. of Expl. Geophys., 2132–2135.

Symes, W. W., and Carazzone, J. J., 1991, Velocity inversion by differential semblance optimization: Geophysics, **56**, 654–663.

Woodward, M. J., 1992, Wave-equation tomography: Geophysics, **57**, 15–26.

Yilmaz, O., 1979, Prestack partial migration: Ph.D. thesis, Stanford University. URL `http://sepwww.stanford.edu/oldreports/sep18/index.html`.

APPENDIX A

THE SCATTERING OPERATOR

Imaging by wavefield extrapolation (WE) is based on recursive continuation of wavefields $\mathcal{U}$ from a given depth level to the next by means of an extrapolation operator **E**. Within every extrapolation slab, we can write that

$$\mathcal{U}_{z+\Delta z} = \mathbf{E}_z \left[\mathcal{U}_z \right], \tag{A-1}$$

where $\mathcal{U}_z$ is the wavefield at the top of the slab, and $\mathcal{U}_{z+\Delta z}$ is the wavefield at the bottom of the slab. The operator **E** involves a spatially-dependent phase shift described by:

$$\mathbf{E}_z \left[\right] = e^{ik_z \Delta z}, \tag{A-2}$$

where k_z represents the depth wavenumber, and Δz the wavefield extrapolation depth step. The relation (A-1) corresponds to the analytical solution of the differential equation

$$\mathcal{U}'(z) = ik_z \mathcal{U}(z) \tag{A-3}$$

which describes depth extrapolation of monochromatic plane waves (Claerbout, 1985). The $'$ sign represents a derivative with respect to the depth z. The depth wavenumber k_z is given by the one-way wave equation, also known as the single square root (SSR) equation

$$k_z = \sqrt{\omega^2 s^2 - |\mathbf{k}|^2}, \tag{A-4}$$

where ω is the temporal frequency, s is the laterally variable slowness of the medium, and $\mathbf{k}$ is the horizontal wavenumber. We use the laterally variable s and the horizontal wavenumber $\mathbf{k}$ in equation (A-4) just for conciseness, although such a notation not mathematically correct in laterally varying media.

Since downward continuation by Fourier-domain phase shift can be applied for slowness models that only vary with depth, we need to split the operator $\mathbf{E}$ into two parts: a constant slowness *continuation operator* applied in the $\omega - \mathbf{k}$ domain, which accounts for the propagation in depth, and a *screen operator* applied in the $\omega - \mathbf{x}$ domain, which accounts for the wavefield perturbations due to the lateral slowness variations. In essence, we approximate the vertical wavenumber k_z with its constant slowness counterpart k_{z0}, corrected by a term describing the spatial variability of the slowness function (Ristow and Ruhl, 1994).

Furthermore, we can separate the depth wavenumber k_z into two components, one which corresponds to the background medium $\widetilde{k}_z$ and one which corresponds to a perturbation of the medium:

$$k_z = \widetilde{k}_z + \Delta k_z \; . \tag{A-5}$$

In a first-order approximation, we can relate those two depth wavenumbers by a Taylor series expansion:

$$\begin{aligned} k_z &\approx \widetilde{k}_z + \left.\frac{dk_z}{ds}\right|_{s=\tilde{s}} (s - \tilde{s}) && \text{(A-6)} \\ &\approx \widetilde{k}_z + \omega \frac{\omega \tilde{s}}{\sqrt{\omega^2 \tilde{s}^2 - |\mathbf{k}|^2}} (s - \tilde{s}) \; , && \text{(A-7)} \end{aligned}$$

where $s(z, \mathbf{x})$ is the slowness corresponding to the perturbed medium, and $\tilde{s}(z, \mathbf{x})$ is the background slowness.

Within any depth slab, we can extrapolate the wavefield from the top either in the perturbed or in the background medium. The wavefields at the bottom of the slab, $\widetilde{\mathcal{U}}_{z+\Delta z} = \mathcal{U}_z e^{i\widetilde{k}_z \Delta z}$ and $\mathcal{U}_{z+\Delta z} = \mathcal{U}_z e^{ik_z \Delta z}$ are related by the relation

$$\mathcal{U}_{z+\Delta z} \approx \widetilde{\mathcal{U}}_{z+\Delta z} e^{i \Delta k_z \Delta z} \; . \tag{A-8}$$

Equation (A-8) is a direct statement of the Rytov approximation (Lo and Inderweisen, 1994), since the wavefields at the bottom of the slab correspond to different phase shifts related by a linear equation.

The wavefield perturbation $\Delta\mathcal{V}$ at the bottom of the slab is obtained by subtracting the background wavefield $\widetilde{\mathcal{U}}$ from the perturbed wavefield $\mathcal{U}$:

$$\begin{aligned}
\Delta\mathcal{V}_{z+\Delta z} &\approx \mathcal{U}_{z+\Delta z} - \widetilde{\mathcal{U}}_{z+\Delta z} && \text{(A-9)}\\
&\approx \left(e^{i\Delta k_z \Delta z} - 1\right)\widetilde{\mathcal{U}}_{z+\Delta z} && \text{(A-10)}\\
&\approx e^{i\widetilde{k}_z \Delta z}\left(e^{i\left.\frac{dk_z}{ds}\right|_{s=\tilde{s}}\Delta s_z \Delta z} - 1\right)\widetilde{\mathcal{U}}_z, && \text{(A-11)}
\end{aligned}$$

where $\Delta s = s - \tilde{s}$ is the perturbation between the correct and the background slownesses at depth z.

In operator form we can write

$$\Delta\mathcal{V}_{z+\Delta z} = \mathbf{E}_z\left[\mathbf{R}_z\left(\widetilde{\mathcal{U}}_z\right)\left[\Delta s_z\right]\right], \tag{A-12}$$

where $\mathbf{E}_z$ represents the downward continuation operator at depth z, and $\mathbf{R}_z$ represents the *Rytov* scattering operator which is dependent on the background wavefield $\widetilde{\mathcal{U}}_z$ and the slowness perturbation Δs_z at that depth level:

$$\mathbf{R}_z\left(\widetilde{\mathcal{U}}_z\right)\left[\Delta s_z\right] = \left(e^{i\left.\frac{dk_z}{ds}\right|_{s=\tilde{s}}\Delta s_z \Delta z} - 1\right)\widetilde{\mathcal{U}}_z\,. \tag{A-13}$$

In this approximation, we assume that the scattered wavefield is generated only by the background wavefield and we ignore all multi-scattering effects. For the Born approximation (Lo and Inderweisen, 1994), we further assume that the wavefield differences are small, such we can linearize the exponential according to the relation $e^{i\Delta\phi} \approx 1 + i\Delta\phi$. With this new approximation, the expression for the downward-continued scattered wavefield becomes:

$$\Delta\mathcal{V}_{z+\Delta z} \approx e^{i\widetilde{k}_z \Delta z}\left(i\left.\frac{dk_z}{ds}\right|_{s=\tilde{s}}\Delta s_z \Delta z\right)\widetilde{\mathcal{U}}_z. \tag{A-14}$$

In operator form, we can write the scattered wavefield at z as

$$\Delta\mathcal{V}_{z+\Delta z} = \mathbf{E}_z\left[\mathbf{S}_z\left(\widetilde{\mathcal{U}}_z\right)\left[\Delta s_z\right]\right] \tag{A-15}$$

where $\mathbf{E}_z$ represents the downward continuation operator at depth z, and $\mathbf{S}_z$ represents the *Born* scattering operator which is dependent on the background wavefield and operates on the slowness perturbation at that depth level.

The linear scattering operator $\mathbf{S}$ is a mixed-domain operator similar to the extrapolation operator $\mathbf{E}$. This operator depends on the background wavefield and background slowness by the expression:

$$\mathbf{S}_z\left(\widetilde{\mathcal{U}}_z\right)\left[\Delta s_z\right] \approx i\,\left.\frac{dk_z}{ds}\right|_{s=\tilde{s}} \Delta z \Delta s_z \widetilde{\mathcal{U}}_z\,. \tag{A-16}$$

In practice, we can implement the scattering operator described by equation (A-16) in different ways.

- One option is to implement the Born operator (A-16) in the space domain using an expansion (Huang et al., 1999) like

$$\left.\frac{dk_z}{ds}\right|_{s=\tilde{s}} \approx \omega\left(1+\frac{1}{2}\left[\frac{|\mathbf{k}|}{\omega\tilde{s}}\right]^2+\frac{3}{8}\left[\frac{|\mathbf{k}|}{\omega\tilde{s}}\right]^4+\frac{5}{16}\left[\frac{|\mathbf{k}|}{\omega\tilde{s}}\right]^6+\frac{35}{128}\left[\frac{|\mathbf{k}|}{\omega\tilde{s}}\right]^8+\ldots\right). \tag{A-17}$$

  In practice, the summation of the terms in equation (A-17) involves forward and inverse Fast Fourier Transforms (FFT and IFT) and multiplication in the space domain with the spatially variable $\tilde{s}$:

$$\Delta\mathcal{V}_z = i\omega\Delta z\Delta s_z\left[1+\sum_{j=1,\ldots} c_j \frac{1}{(\omega\tilde{s})^{2j}}\,\mathtt{IFT}\left[|\mathbf{k}|^{2j}\,\mathtt{FFT}\left[\widetilde{\mathcal{U}}_z\right]\right]\right], \tag{A-18}$$

  where $c_j = \frac{1}{2}, \frac{3}{8}, \ldots$

- Another option is to implement the Born operator (A-16) in the Fourier domain relative to the constant reference slowness in any individual slab. In this case, we can write

$$\left.\frac{dk_z}{ds}\right|_{s=s_o} \approx \omega\frac{\omega s_o}{\sqrt{\omega^2 {s_o}^2-(1-i\eta)^2|\mathbf{k}|^2}}\,, \tag{A-19}$$

  where η as a damping parameter which avoids division by zero (de Hoop et al., 1996). In practice, the implementation of equation (A-19) involves forward and inverse Fast Fourier

Transforms (FFT and IFT):

$$\Delta \mathcal{V}_z = i\,\Delta z\ \texttt{IFT}\left[\left.\frac{dk_z}{ds}\right|_{s=s_o}\ \texttt{FFT}\left[\widetilde{\mathcal{U}}_z \Delta s_z\right]\right]. \tag{A-20}$$

APPENDIX B

DIFFERENTIAL IMAGE PERTURBATIONS

A differential image perturbation is computed using a residual migration operator (**K**) using a relation like

$$\Delta\mathcal{R} \approx \mathbf{K}^{'}\Big|_{\rho=1}\left[\widetilde{\mathcal{R}}\right]\Delta\rho\ . \tag{B-1}$$

The operator **K** depends on the scalar parameter ρ which is a ratio of the velocity to which we residually migrate and the background velocity. The background image corresponds to $\rho = 1$.

Using the chain rule of differentiation, we can write

$$\Delta\mathcal{R} \approx \frac{d\mathbf{K}}{dk_z}\frac{dk_z}{d\rho}\Big|_{\rho=1}\left[\widetilde{\mathcal{R}}\right]\Delta\rho\ , \tag{B-2}$$

where k_z is the depth wavenumber defined for PSRM.

Equation (B-2) offers the possibility to build the image perturbation directly, by computing three elements: the derivative of the image with respect to the depth wavenumber, and two weighting functions, one for the derivative of the depth wavenumber with respect to the velocity ratio parameter (ρ), and the other one for the magnitude of the $\Delta\rho$ perturbation from the reference to the improved image.

Firstly, the image derivative in the Fourier domain, $\frac{d\mathbf{K}}{dk_z}$, is straightforward to compute in the space domain as

$$\frac{d\mathbf{K}}{dk_z}\Big|_{\rho=1}\left[\widetilde{\mathcal{R}}\right] = -iz\widetilde{\mathcal{R}}\ . \tag{B-3}$$

The derivative image is nothing but the imaginary part of the migrated image, scaled by depth.

Secondly, we can obtain the weighting representing the derivative of the depth wavenumber with respect to the velocity ratio parameter, $\frac{dk_z}{d\rho}\Big|_{\rho=1}$, starting from the double square root (DSR) equation

written for prestack Stolt residual migration (Sava, 2003):

$$\begin{aligned} k_z &= k_{z_s} + k_{z_r} \\ &= \frac{1}{2}\sqrt{\rho^2\mu^2 - |\mathbf{k}_s|^2} + \frac{1}{2}\sqrt{\rho^2\mu^2 - |\mathbf{k}_r|^2}\,, \end{aligned}$$

where μ is given by the expression:

$$\mu^2 = \frac{\left[4\left(k_{z0}\right)^2 + (\mathbf{k}_r - \mathbf{k}_s)^2\right]\left[4\left(k_{z0}\right)^2 + (\mathbf{k}_r + \mathbf{k}_s)^2\right]}{16{k_{z0}}^2}\,. \tag{B-4}$$

The derivative of k_z with respect to ρ is

$$\frac{dk_z}{d\rho} = \rho\left(\frac{\mu^2}{4k_{z_s}} + \frac{\mu^2}{4k_{z_r}}\right)\,, \tag{B-5}$$

therefore

$$\left.\frac{dk_z}{d\rho}\right|_{\rho=1} = \frac{\mu^2}{2\sqrt{\mu^2 - |\mathbf{k}_s|^2}} + \frac{\mu^2}{2\sqrt{\mu^2 - |\mathbf{k}_r|^2}}\,. \tag{B-6}$$

LIST OF FIGURES

Born approximation.

5 A schematic description of our method for computing linearized image perturbations, depicting images on the vertical axis function of velocity on the horizontal axis. The dashed line corresponds to image changes described by residual migration with various values of the velocity ratio parameter (ρ). The straight solid line corresponds to the linearized image perturbation computed with an image gradient operator applied to the reference image scaled at every point by the difference of the velocity ratio parameter $\Delta\rho$.

6 Comparison of slowness backprojections using the WEMVA operator applied to image perturbations computed with the differential image perturbation operator (b,d) and as the result of the forward WEMVA operator applied to a known slowness perturbation (c,e). Panel (a) depicts the background image corresponding to the background slowness. Despite the fact that the slowness perturbation is large (20%), the image perturbations in panels (b) and (c) and the fat rays in panels (d) and (e) are practically identical, both in shape and in magnitude.

7 Comparison of common-image gathers for image perturbations obtained as a difference between two migrated images (c), as the result of the forward WEMVA operator applied to the known slowness perturbation (d), and as the result of the differential image perturbation operator applied to the background image (e). Panel (a) depicts the background image corresponding to the background slowness, and panel (b) depicts an improved image obtained from the background image using residual migration. Despite the fact that the slowness perturbation is large (50%), the image perturbations in panels (b) and (c) are identical within numeric precision.

8 WEMVA applied to a simple model with flat reflectors. The background image (a), the image updated after one non-linear iteration (b), and the image computed with the correct slowness (c).

9 WEMVA applied to a simple model with flat reflectors. The zero-offset of the image per-

turbation (a), the slowness update after the first non-linear iteration (b), and the convergence curve of the first linear iterations (c).

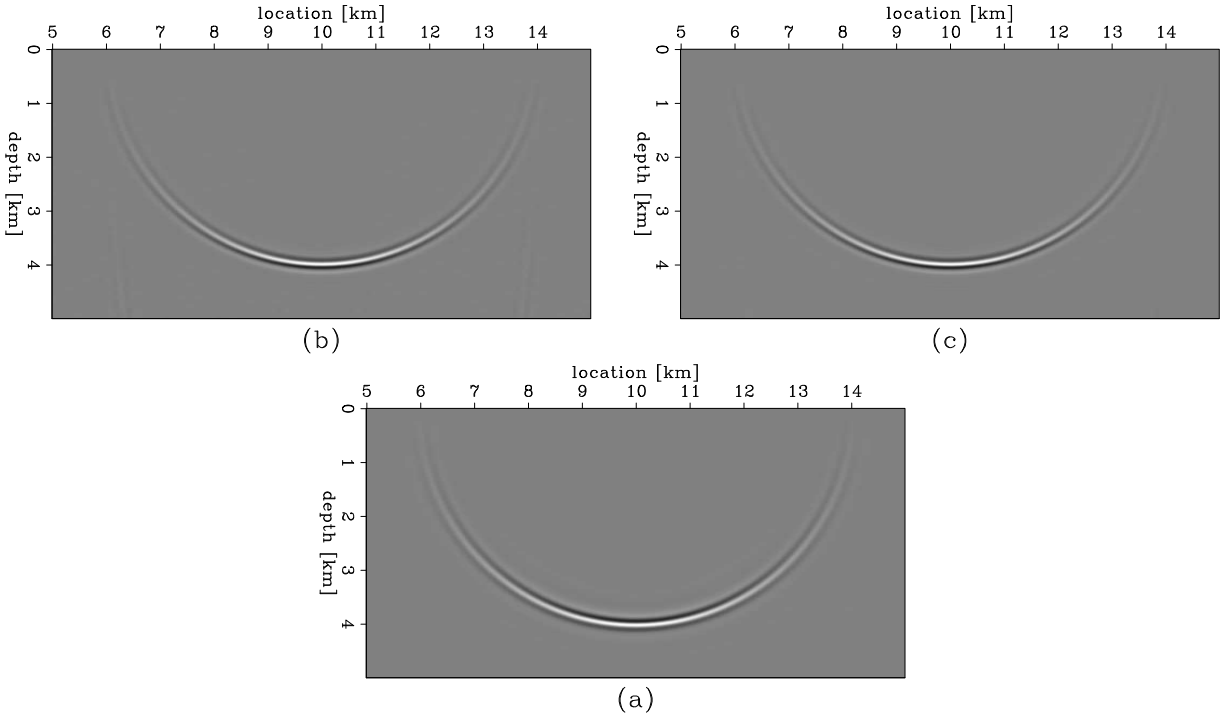
location [km]
5 6 7 8 9 10 11 12 13 14
0 1 2 3 4
depth [km]
(b)
location [km]
5 6 7 8 9 10 11 12 13 14
0 1 2 3 4
depth [km]
(c)
location [km]
5 6 7 8 9 10 11 12 13 14
0 1 2 3 4
depth [km]
(a)

Figure 1.

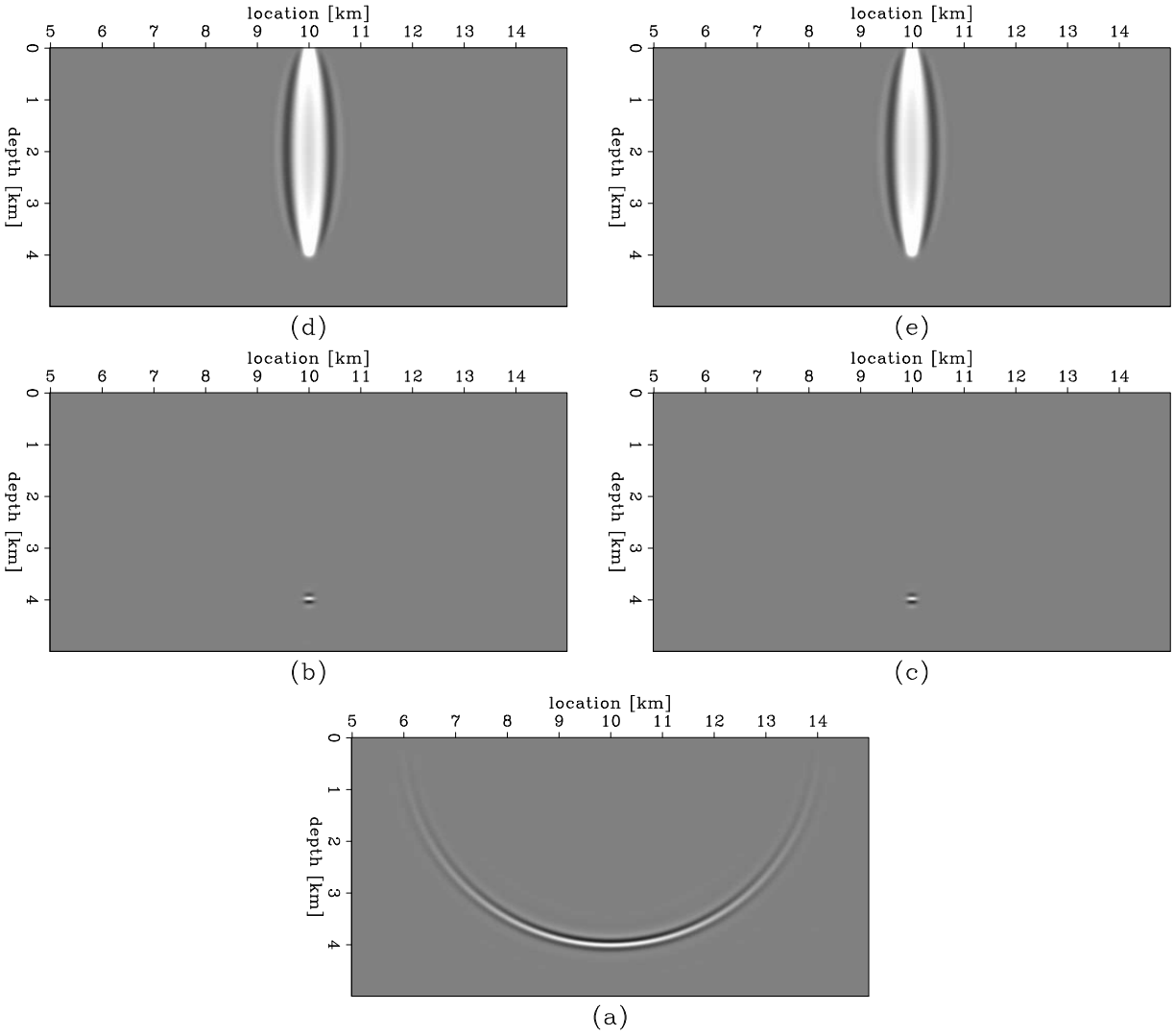

Figure 2.

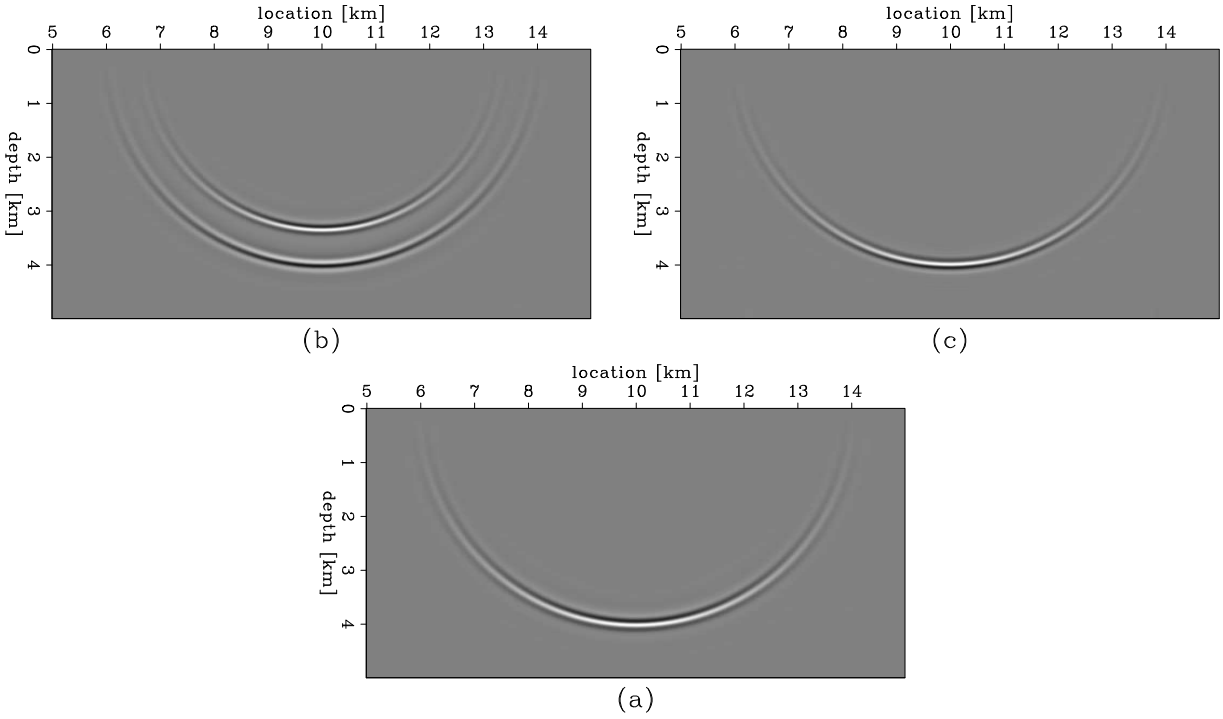
location [km]
5 6 7 8 9 10 11 12 13 14
depth [km]
0 1 2 3 4
(b)
location [km]
5 6 7 8 9 10 11 12 13 14
depth [km]
0 1 2 3 4
(c)
location [km]
5 6 7 8 9 10 11 12 13 14
depth [km]
0 1 2 3 4
(a)

Figure 3.

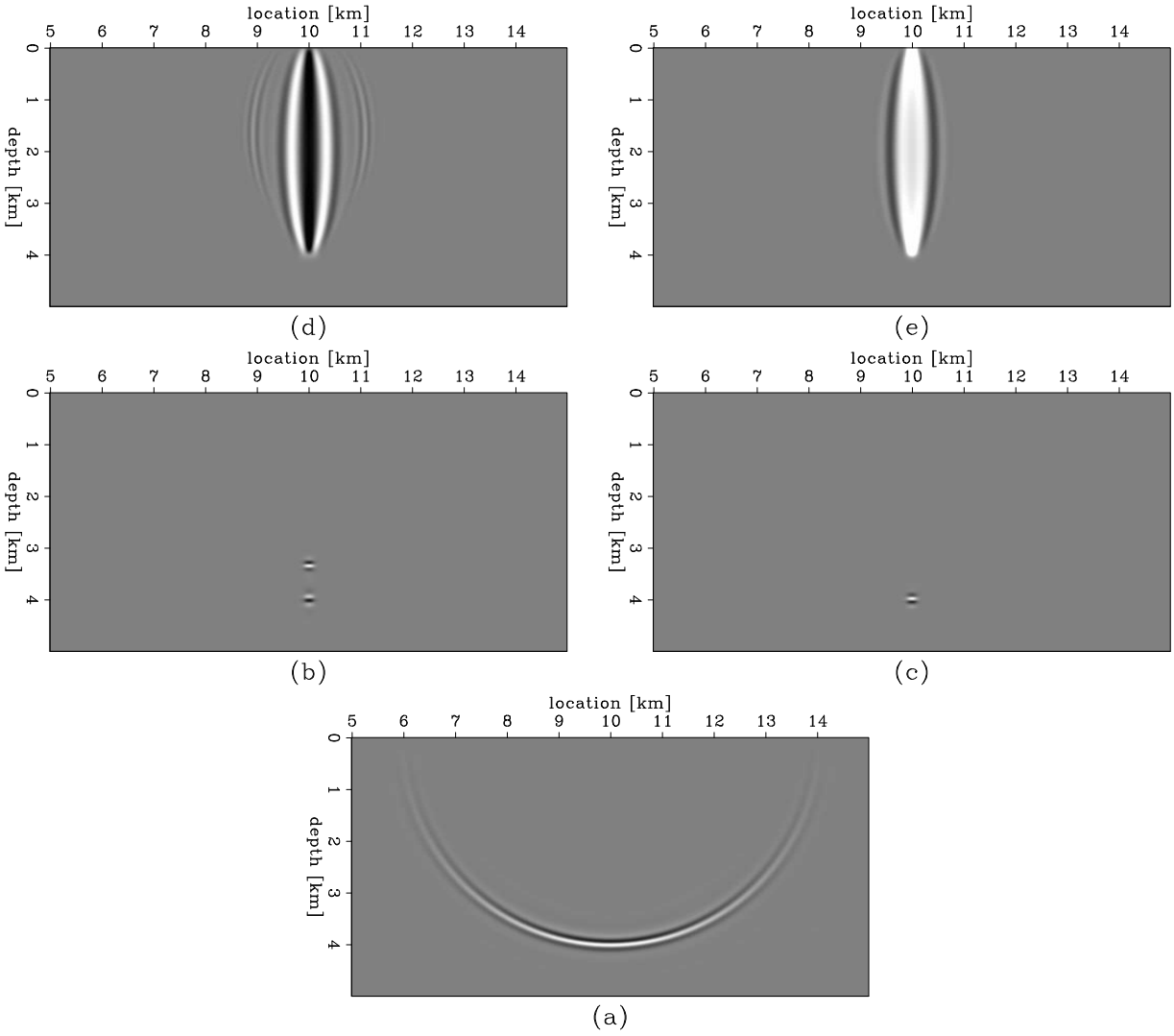

Figure 4.

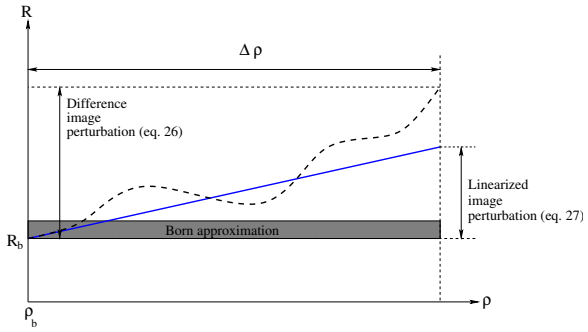
R
Δ ρ
Difference
image
perturbation (eq. 26)
Linearized
image
perturbation (eq. 27)
Born approximation
R_b
ρ
ρ_b

Figure 5.

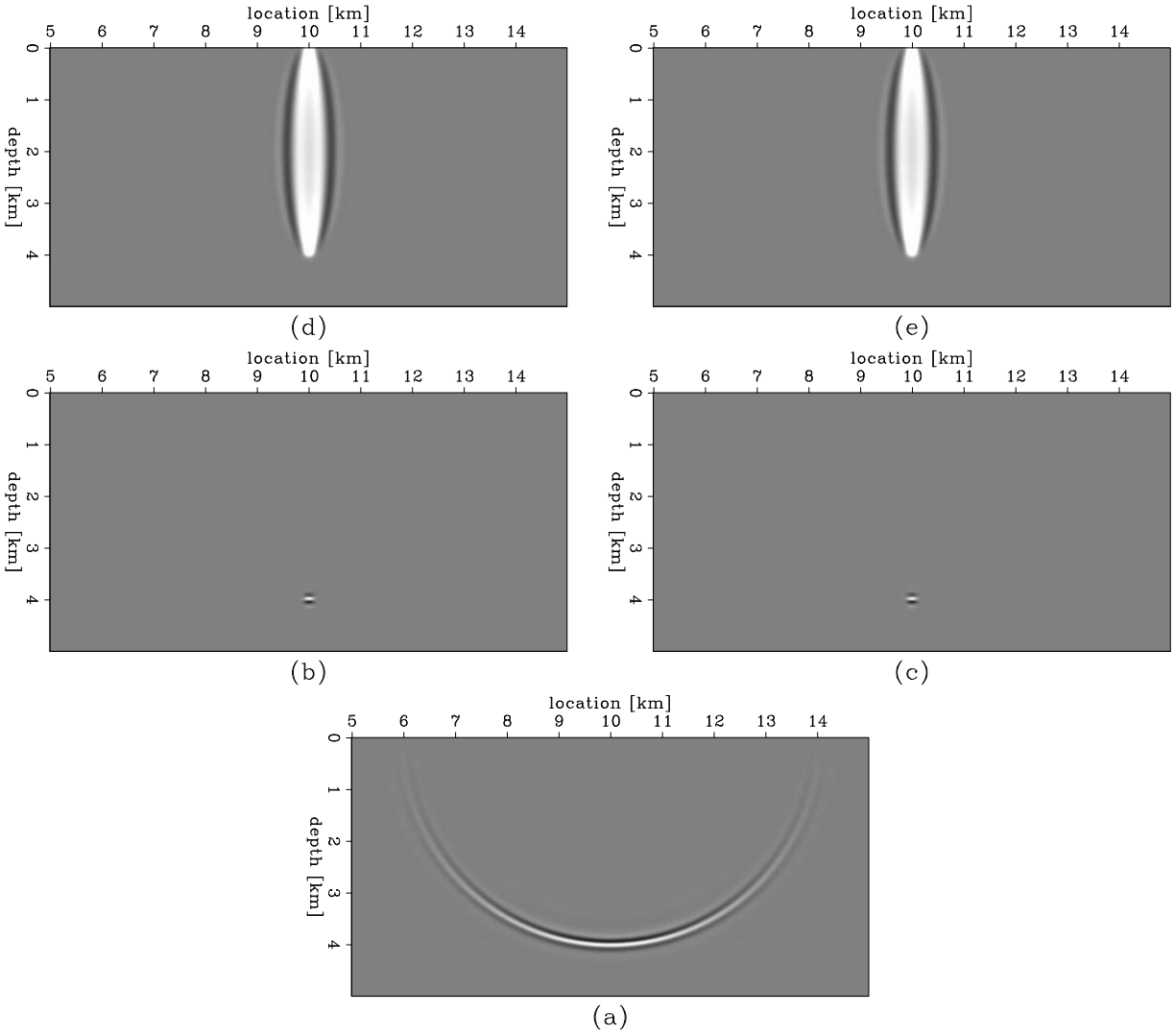

Figure 6.

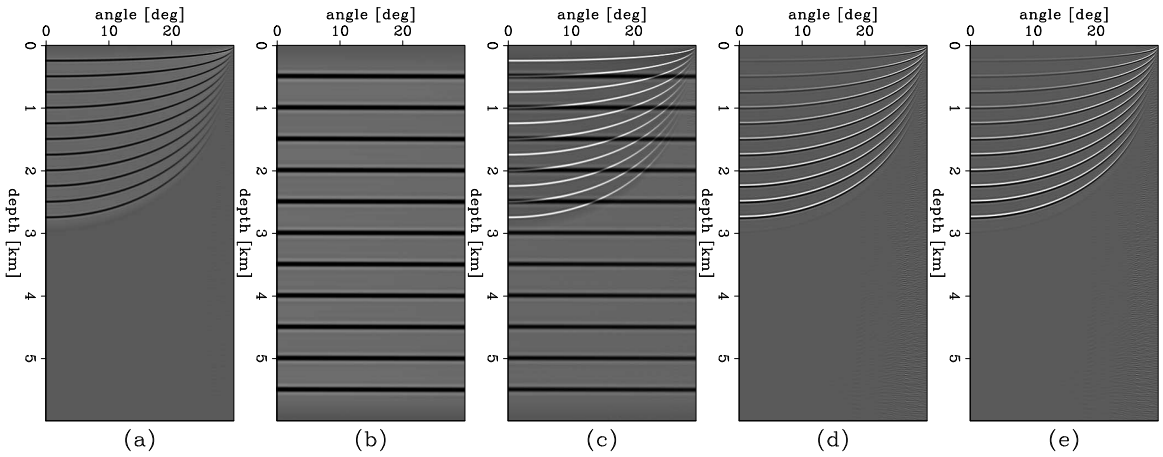

Figure 7.

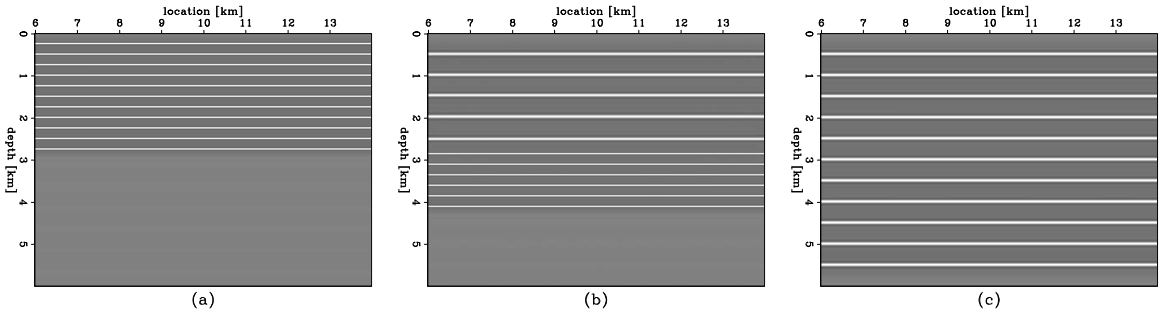
location [km]
6 7 8 9 10 11 12 13
depth [km]
0 1 2 3 4 5
(a)
location [km]
6 7 8 9 10 11 12 13
depth [km]
0 1 2 3 4 5
(b)
location [km]
6 7 8 9 10 11 12 13
depth [km]
0 1 2 3 4 5
(c)

Figure 8.

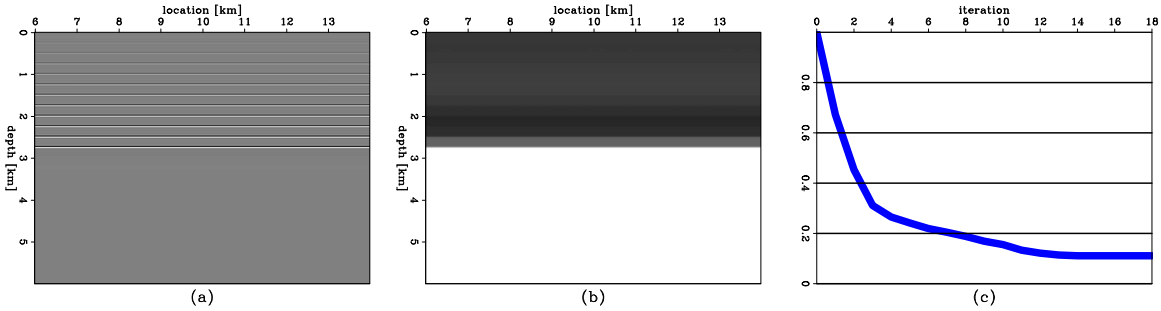

Figure 9.